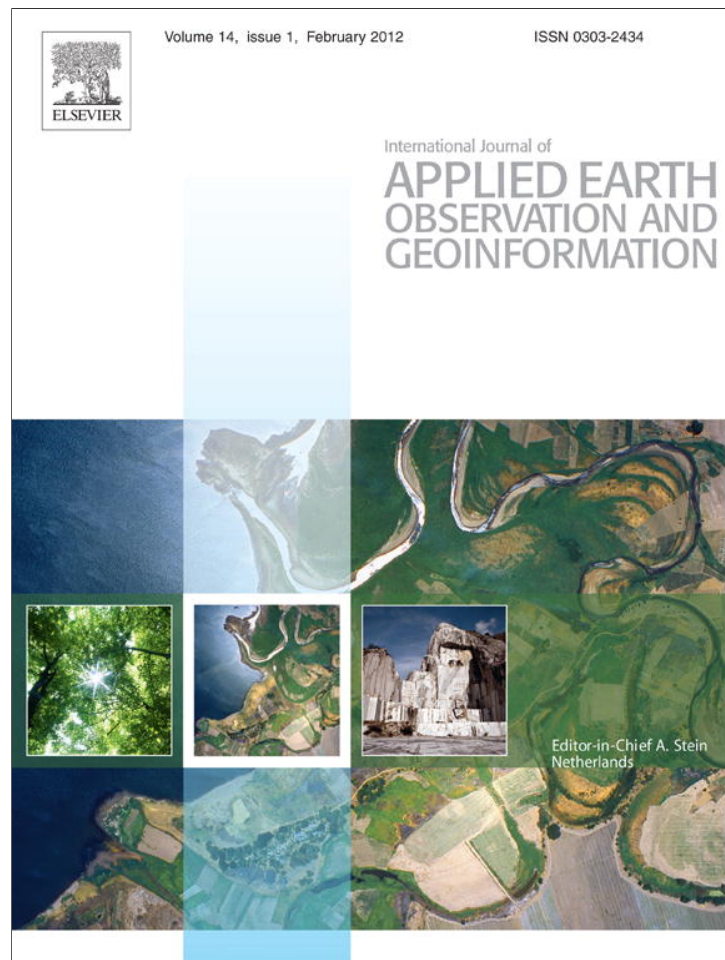


Provided for non-commercial research and education use.
Not for reproduction, distribution or commercial use.



(This is a sample cover image for this issue. The actual cover is not yet available at this time.)

This article appeared in a journal published by Elsevier. The attached copy is furnished to the author for internal non-commercial research and education use, including for instruction at the authors institution and sharing with colleagues.

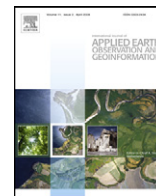
Other uses, including reproduction and distribution, or selling or licensing copies, or posting to personal, institutional or third party websites are prohibited.

In most cases authors are permitted to post their version of the article (e.g. in Word or Tex form) to their personal website or institutional repository. Authors requiring further information regarding Elsevier's archiving and manuscript policies are encouraged to visit:

<http://www.elsevier.com/copyright>

Contents lists available at [SciVerse ScienceDirect](http://www.sciencedirect.com)

International Journal of Applied Earth Observation and Geoinformation

journal homepage: www.elsevier.com/locate/jag

Land cover mapping with emphasis to burnt area delineation using co-orbital ALI and Landsat TM imagery

George P. Petropoulos^{a,*}, Charalambos C. Kontoes^b, Iphigenia Keramitsoglou^b^a University of Aberystwyth, Institute of Geography and Earth Sciences, Ceredigion SY23 2EJ, Wales, United Kingdom^b Institute for Space Applications and Remote Sensing, National Observatory of Athens, I. Metaxa and Vas. Pavlou St, Penteli, SY23 2DB Athens, Greece

ARTICLE INFO

Article history:

Received 2 February 2011

Received in revised form 15 February 2012

Accepted 17 February 2012

Keywords:

Burnt area mapping

Landsat TM

EO-1 Advanced Land Imager (ALI)

Support Vector Machines

Artificial Neural Networks

Maximum Likelihood

Greece

ABSTRACT

In this study, the potential of EO-1 Advanced Land Imager (ALI) radiometer for land cover and especially burnt area mapping from a single image analysis is investigated. Co-orbital imagery from the Landsat Thematic Mapper (TM) was also utilised for comparison purposes. Both images were acquired shortly after the suppression of a fire occurred during the summer of 2009 North-East of Athens, the capital of Greece. The Maximum Likelihood (ML), Artificial Neural Networks (ANNs) and Support Vector Machines (SVMs) classifiers were parameterised and subsequently applied to the acquired satellite datasets. Evaluation of the land use/cover mapping accuracy was based on the error matrix statistics. Also, the McNemar test was used to evaluate the statistical significance of the differences between the approaches tested. Derived burnt area estimates were validated against the operationally deployed Services and Applications For Emergency Response (SAFER) Burnt Scar Mapping service.

All classifiers applied to either ALI or TM imagery proved flexible enough to map land cover and also to extract the burnt area from other land surface types. The highest total classification accuracy and burnt area detection capability was returned from the application of SVMs to ALI data. This was due to the SVMs ability to identify an optimal separating hyperplane for best classes' separation that was able to better utilise ALI's advanced technological characteristics in comparison to those of TM sensor. This study is to our knowledge the first of its kind, effectively demonstrating the benefits of the combined application of SVMs to ALI data further implying that ALI technology may prove highly valuable in mapping burnt areas and land use/cover if it is incorporated into the development of Landsat 8 mission, planned to be launched in the coming years.

© 2012 Elsevier B.V. All rights reserved.

1. Introduction

Land cover is a fundamental variable of the Earth's system strongly connected with many parts of the human and physical environment. Changes in land cover dynamics is regarded as the most important variable of global change affecting ecological systems (Otukey and Blaschke, 2010). Wildland fires are a major ecological disturbance factor of natural ecosystems threatening environmental systems and infrastructure worldwide, affecting the distribution of land use and land cover (e.g. FAO, 2001; Petropoulos et al., 2011a). Those have a major impact to the economy of an affected country, influencing also the broader economies through the destruction occurred in marketable assets (Sifakis et al., 2011). Thus, the extraction of information on past fire events including accurate mapping of burnt areas is underlined as a matter of key

importance and priority for future attention by both environmental scientists and policy makers (Giglio et al., 2006; Kontoes et al., 2009).

The progress in earth observation technology of the past three decades or so has allowed monitoring from space the landscape destruction caused by wildland fires. Several algorithms applied to satellite imagery acquired at various spatial, spectral and temporal resolutions have shown promise in delineating the burnt areas (e.g. Dixon and Candade, 2008; Petropoulos et al., 2010a,b). Satellite image classification is generally regarded as the most commonly used approach in deriving information on the pattern and the spatial distribution of land cover and of its changes (Mathur and Foody, 2008). It is also one of the most widely used approaches in mapping burnt areas (Kokaly et al., 2007; Petropoulos et al., 2011a). Numerous image classifiers have been developed, a recent comprehensive review of which can be found in Lu and Weng (2007). The selection of the suitable classifier as well as of the appropriate spectral bands- original or derived- are both crucial for the success of the classification. Limitations of previous generation satellite sensors with respect to their suitability for burnt area mapping

* Corresponding author. Tel.: +44 01970 621861; fax: +44 01970 621861.

E-mail addresses: petropoulos.george@gmail.com, george.petropoulos@aber.ac.uk (G.P. Petropoulos).

have been extensively discussed and identified (e.g. Quintano et al., 2006).

At present we are in an era characterized by the development of new spaceborne sensing. Those aim to replace existing radiometers such of Landsat series, yet ensuring the continuity of observations so that their archive can be maintained (Thenkabail et al., 2004). The need to evaluate specifically the capability of new generation remote sensing sensors combined with contemporary techniques with respect to land use and land cover and/or burnt area mapping has been pointed out as a direction of critical importance and priority (Silva et al., 2005; Roy and Boschetti, 2009). In this context, the Earth Observing-1 (EO-1) mission launched in November 2000 under United States National Aeronautics and Space Administration (NASA's) New Millennium Program, aims at developing and validating instruments and technologies for space-based Earth observation with unique spatial, spectral and temporal characteristics not previously available (Pu et al., 2005). The Advanced Land Imager (ALI) is one of three operational instruments on board the EO-1 platform (Ungar et al., 2003). ALI is a multispectral sensor included in EO-1 with the intention to be used specifically in evaluating new technologies for the development of the future Landsat 8.

The use of ALI data has so far been explored in various applications related to geology (Hubbard and Crowley, 2005; Deller, 2006), vegetation mapping (Pimstein et al., 2009; Helmer et al., 2010) as well as lake water dissolved organic matter (Chen et al., 2009). Many investigators have also examined ALI's potential comparative to that of Landsat TM/ETM+ (e.g. Thenkabail et al., 2004; Neuenschwander et al., 2005; Deller, 2006; Helmer et al., 2010). However, to our knowledge, not adequate attention seems to have been paid in examining ALI's capability in land cover mapping with emphasis to burnt area delineation, particularly in comparison to other sensors. Given that Landsat TM/ETM+ performance in both land cover and burnt area mapping has been extensively examined using diverse classification approaches (e.g. Dixon and Candade, 2008; Petropoulos et al., 2010a,b), it would be of great interest to examine ALI's potential versus TM/ETM+ for this purpose. Understandably, such a study should be performed in a Mediterranean setting, a fire-prone region (Castillejo-Gonzalez et al., 2009).

In this context, the objective of our study was to identify the capability of ALI to land use/cover and burnt area mapping, based on a single image and a range of pixel-based classification techniques. An additional objective was to evaluate the contribution of the advanced technology incorporated in ALI, namely the role of additional bands as well as the higher signal to noise ratio and increased dynamic range, versus the traditionally used TM imagery in land use/cover and burnt areas mapping. As a case study we used a destructive Mediterranean fire that broke out in August 2009 close to Athens, the capital of Greece, for which near co-orbital ALI and TM images acquired shortly after the fire suppression were available.

2. Experimental set up

2.1. Study site

The study site comprises the area of eastern Attica, located approximately 30 km north-east from the city of Athens. The surface area covered is approximately 220 km², extending approximately from 23°2' to 26°1' East, and from 36°4' to 38°4' North. The region is representative of typical Mediterranean conditions in terms of both landscape structure and land surface cover variation. The terrain varies highly from sea level to approximately 800 m, whereas the vegetation of the area also varies with altitude. The climate of the area is typical Mediterranean,

Table 1
Wavebands and spatial resolution of the ALI and Landsat TM/ETM.

Landsat TM/ETM+		EO-1 ALI	
Band	Range (μm)	Band	Range (μm)
1 (30 m)	0.450–0.520	1p (30 m)	0.432–0.451
2 (30 m)	0.530–0.610	1 (30 m)	0.458–0.511
3 (30 m)	0.630–0.690	2 (30 m)	0.532–0.602
4 (30 m)	0.780–0.900	3 (30 m)	0.632–0.688
		4 (30 m)	0.775–0.805
		4p (30 m)	0.845–0.888
		5p (30 m)	1.200–1.288
5 (30 m)	1.550–1.750	5 (30 m)	1.554–1.725
7 (30 m)	2.090–2.350	7 (30 m)	2.090–2.362
Pan (15 m) ^a	0.520–0.900	Pan (10 m)	0.480–0.690

^a Pan band is not available on the TM sensor. Also the Landsat TM/ETM+ thermal band has not been included in the table.

characterised by hot, dry summers and cool, wet winters, with a long dry period starting in April and lasting until September. At lower elevations, land is covered mainly by sclerophyllous vegetation, sparse vegetation areas and some agricultural land. At higher altitudes, areas are covered mainly by forest of different types as well as transitional woodland/scrubland areas. The study site experienced severe damage from a wildfire outbreak on August 21st, 2009, which was suppressed approximately 3 days later.

2.2. Datasets

ALI is a multispectral sensor onboard EO-1 that follows a sun-synchronous, near-polar orbit with a nominal altitude of 705 km at the equator. ALI acquires data covering a ground swath width of 185 km. The primary characteristics of ALI reflective bands contrasted with those from Landsat TM/ETM+ are listed in Table 1. In comparison to Landsat TM/ETM+, ALI sensor has three additional bands at 30 m spatial resolution and also one panchromatic band at a spatial resolution of 10 m. Furthermore, in comparison to Landsat TM/ETM+, ALI has an increased dynamic range (12 bit vs. 8 bit) and an improved signal-to-noise ratio (SNR). The prototype ALI instrument was found to exceed ETM+ SNR by a factor of 4–8 (CEOS, 2012). Because ALI was developed as a technology demonstration instrument and not as an operational land imager, ALI observations are mission-objeced and programmed.

In our study, near co-orbital satellite imagery from Landsat TM (path: 182, row: 34) and ALI (path: 183, row: 33) over our study region was obtained. Images were acquired at no cost from the United States Geological Survey (USGS) archive (<http://glovis.usgs.gov/>). The acquisition dates of the TM and ALI images were September 3rd, 2009 and August 30th, 2009, respectively. The TM image was acquired as a full long scene in GeoTiff format at Level 1G, meaning that it was radiometrically, geometrically and terrain corrected, the latter meaning that a Digital Elevation Model (DEM) has been employed for topographic accuracy (USGS web site). The ALI image was also received as a full long scene in GeoTIFF format and at L1GST processing level, meaning that it was radiometrically corrected, geometrically resampled and registered to a geographic map projection image with elevation correction applied to the 16-bit integer radiance values. The ALI image was acquired georeferenced to a UTM 34N projection with a WGS84 ellipsoid, whereas the TM image was provided in UTM 35N projection and WGS84 ellipsoid.

In addition to the above datasets, a burnt area map generated in the framework of the Burnt Scar Mapping service (BSM-1) of the Services and Applications For Emergency Response (SAFER) European Commission (EC) project (<http://www.emergencyresponse.eu>) was used for validation

purposes. SAFER is a Research & Development Project aimed at developing in Europe standardized space-based geo-information products, strengthening Europe's capacity to respond to emergency situations. The BSM vector polygon used in our study, was generated by the National Observatory of Athens (NOA) project partner after applying the so-called BSM.NOA processing algorithm (Kontoes et al., 2009). This is a standardised and validated fixed thresholding approach that provided the appropriate accuracy of the delivered burnt area mapping products (Kontoes et al., 2009) currently being used operationally to accurately map burnt areas at European scale. The BSM-1 map was generated using the same Landsat TM image as the one used in this study and was subsequently refined with a very high spatial resolution IKONOS scene of August 26th, 2009.

3. Methodology

Land cover and burnt area mapping was performed by independently applying the Maximum Likelihood (ML, e.g. Richards, 1999), Support Vector Machines (SVMs, Vapnik, 1995) and Artificial Neural Networks (ANNs, e.g. Haykin, 1994) pixel-based classifiers to the ALI and TM images. An overview of the main image processing steps applied is shown in Fig. 1, whilst a brief description of those steps is provided in the following sections.

3.1. Pre-processing

ALI and TM images were imported to ENVI software platform (ITT Visual Information Solutions SA) and Digital Numbers (DNs) were converted to radiance units following the procedure described in the Landsat 7 Science data users handbook for ETM+, and as outlined within Mendenhall et al. (1999) for ALI. Subsequently, the image bands from each sensor were layer stacked to form a single image file corresponding to the imagery acquired from each sensor. For consistency with ALI (Table 1), Landsat TM thermal band was excluded from further analysis. Next, image to image co-registration was performed using the TM image as reference. Subsequently, the two images were further layer-stacked to form a single dataset, after masking out the non-overlapping areas between the two images. To ensure consistency with SAFER validation dataset, the non-commonly covered land surface area was masked out from the SAFER burnt area vector product. Geopositional accuracy fell within the sensor pixel range (RMS ~ 30 m), which was considered satisfactory. Water masking was then applied to the layer-stacked dataset, based on a single image thresholding approach using TM band 1 (Kontoes et al., 2009). Atmospheric correction was decided not to be performed, following Datt et al. (2003) and Pengra et al. (2007) who reported that it was not necessary to atmospherically correct image data for a single observation. Furthermore, as the burnt area estimate of SAFER had been derived from the analysis of the analysis of TM imagery at L1T processing level, no further correction was applied to our TM and ALI images. This also ensured consistency in our comparisons and guaranteed the integrity and validity of our analysis. The pre-processed images were classified using the different pixel-based classifiers, as will be described next.

3.2. Image classification

Supervised image classification using Maximum Likelihood (ML), Support Vector Machines (SVMs) and Artificial Neural Network (ANNs) methodologies was applied to ALI and TM images for mapping land use/land cover and extracting burnt area. Bearing in mind the differences in the operation between the three classifiers, it deemed interesting to examine how their different properties

take advantage of the ALI's improved instrument technology in comparison to TM's in mapping land use/cover and extracting the burnt areas. This was considered to be also particularly interesting in the context of new technologies evaluation for the development of the future Landsat 8 mission for which ALI has been specifically developed.

Each of the selected classifiers was subsequently parameterised and then applied to the ALI and TM images following three steps. Firstly, the classification key was formulated, consisting of the classes "agricultural areas", "artificial surfaces", "forests", "semi-natural vegetation" and "burnt area". The decision to use this classification scheme was based primarily on photo-interpretation of the ALI panchromatic imagery (10m spatial resolution). Decision was also assisted by our familiarity with the study area from previous work conducted in the same region (Petropoulos et al., 2011a). Secondly, training pixels representative of each class included in our classification scheme were collected from the ALI and the TM images. Selection of the training sites was guided by photo-interpretation of the ALI panchromatic imagery, as well as targeted field visits conducted during September 2009. Training pixels were determined carefully and were selected from regions appearing homogeneous regions at the sensors' observational scale. Approximately 115 pixels of each class included in our classification scheme (a total of approximately 665 pixels) were identified as training data. Evaluation of the suitability of the selected training pixels was performed by examining their statistical separability. This was also done in ENVI, by computing both the Jeffries-Matusita and the Transformed Divergence separability indices (ENVI User's Guide, 2008). A separability index for all class pairs was reported as always higher than 1.24 and 1.84 for the TM and the ALI imagery respectively. Those results suggested generally a very good separability between the compared spectral pairs representing the different classes. Thirdly, using the previously collected training points selected classifiers were parameterised and implemented one by one to the ALI and the TM images. To ensure consistency, the same training points were used when each classifier was applied to the ALI and TM images. Next, a brief explanation of the three algorithms functionality and details concerning their parameterisation is provided.

3.2.1. Maximum Likelihood

Maximum likelihood classification assumes that the statistics for each class in each band are normally distributed and calculates the probability that a given pixel belongs to a specific class. ML estimates the means and variances of the classes directly from the training data, and then those are used to be computed the probabilities. ML considers not only the mean or average values in assigning classification, but also the variability of brightness values in each class. The maximum likelihood decision rule is based on the probability that a pixel belongs to a particular class. If the highest probability is smaller than a threshold specified, the image pixel remains unclassified. In ENVI maximum likelihood classification is implemented by calculating the discriminant functions for each pixel in the image shown in Eq. (1), below (ENVI User's Guide, 2008):

$$g_i(x) = \ln p(w_i) - \frac{1}{2} \ln |\Sigma_i| - \frac{1}{2} (x - m_i)^t \Sigma_i^{-1} (x - m_i), \quad (1)$$

where i is the class; x is the n -dimensional data (where n is the number of bands); $p(w_i)$ is the probability of class w_i occurs in the image and is assumed the same for all classes; $|\Sigma_i|$ is the determinant of the covariance matrix of the data in class w_i ; Σ_i^{-1} is its inverse matrix; and m_i is the mean vector.

The basic equation assumes that these probabilities are equal for all classes, and that the input bands have normal distributions.

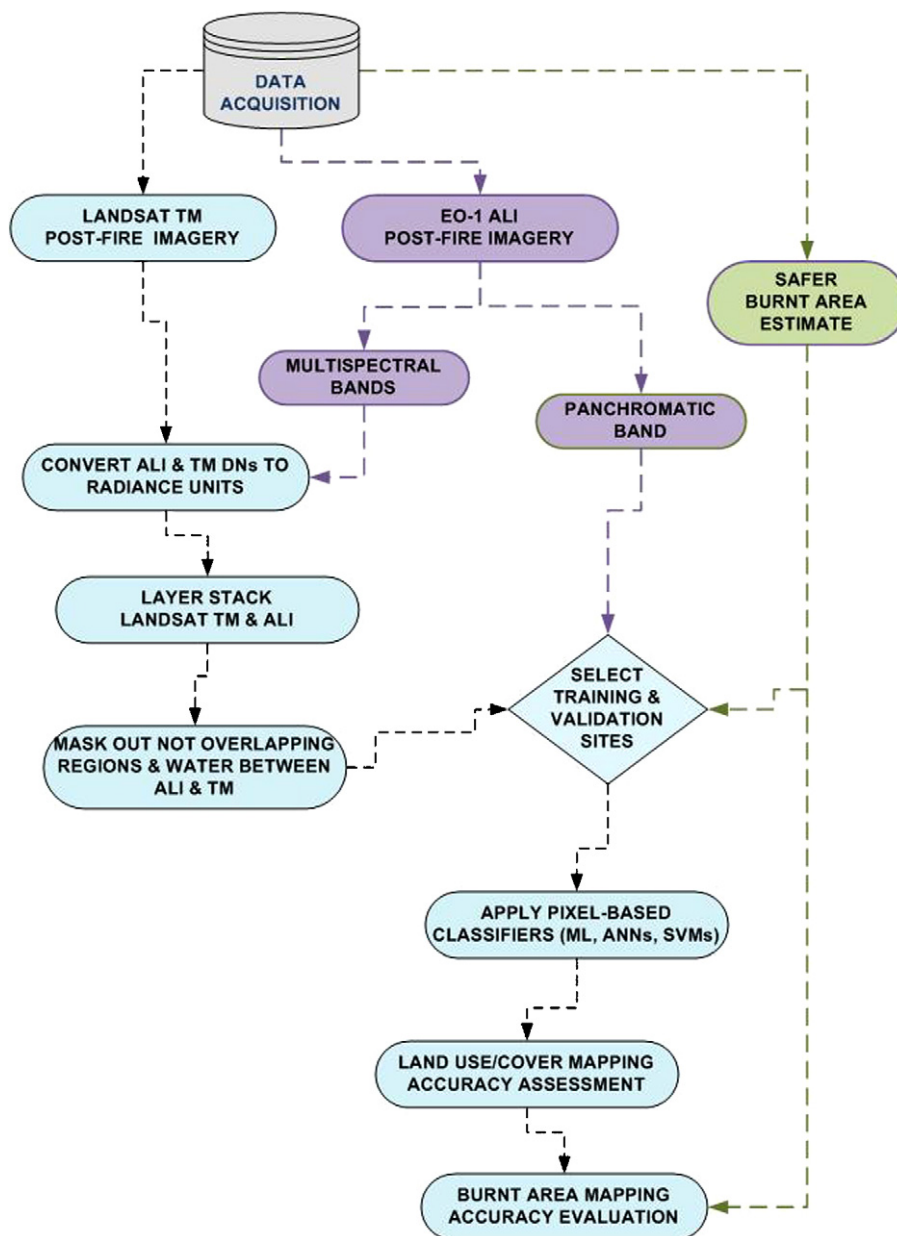


Fig. 1. Flowchart of the overall methodology followed.

The maximum likelihood algorithm assumes that the histograms of the bands of data have normal distributions. An important advantage of this method in comparison to other parametric classifiers of its kind is that it provides an estimate of overlap areas based on statistics. Other parametric classifiers (such as the parallel piped) use only maximum and minimum pixel values to classify image pixels. ML has generally shown to provide high classification accuracy results, as long as accurate training data is provided (ENVI User's Guide, 2008). In the present study, for both the ALI and TM images, ML was parameterised in ENVI using all the training points selected previously (Section 3.2). A single threshold value for all classes in the classification was set up, using probability threshold value equal to zero, meaning that no pixels lower than this value are classified and also using as a data scale factor one. The scale factor is a division factor used to convert integer scaled reflectance or radiance data into floating-point values.

3.2.2. Support Vector Machines

SVMs is a supervised machine learning technique that performs classification based on the statistical learning theory. Briefly, for the simple case of two classes separation, SVMs operation is based on fitting a hyperplane that provides the best separation between the two classes in a multidimensional feature space. This hyperplane forms essentially the decision surface on which the optimal class separation takes place. Intuitively, the optimal hyperplane is the one that maximizes the distance between the hyperplane and the nearest positive and negative training example, called the margin. Generally, the larger the margin, the lower is the generalisation error of the classifier. From a given set of training data, the optimization problem is solved to find the hyperplane that leads to a sparse solution. Hence, only a subset of the training samples, those that lie on the margin (called "support vectors") are used to define the hyperplane. Thus, often not all the obtainable training examples are used in the design of the separating

hyperplane, and this is a key generalization feature of SVMs in comparison to other non-parametric classifiers. In case of a non-linearly separable input space, kernel function is often used to map the non-linear correlations into a dimensional space. Commonly used kernels include the polynomial, the radial basis function (RBF) and the sigmoid kernels. A recent overview of remote sensing applications using SVM was provided by Mountrakis et al. (2011).

In the present study, multiclass SVMs pair-wise classification strategy was implemented in ENVI. SVMs was applied at the original spatial resolution of 30 m of each imagery acquired. In defining the SVMs feature space all the sensor reflective bands after the end of pre-processing were used (described in Section 3.1). Concerning the kernel-specific parameterisation, also generally very little guidance exists in the literature (e.g. Li and Liu, 2010). The RBF kernel function was used for performing the pair-wise SVMs classification. The rationale for selecting this kernel was guided by the fact that it requires the definition of only a small amount of parameters to run and has also shown to produce generally promising results in other classification-related studies (e.g. Huang et al., 2008; Petropoulos et al., 2011b).

RBF kernel was parameterised based on performing a number of trials of parameters combinations, using classification accuracy as a measure of quality. Such an approach has also been adopted in the past in analogous studies of SVMs implementation (e.g. Kueemmerle et al., 2009; Petropoulos et al., 2011b). In addition, suggestions provided for the parameterization of these values from the ENVI User's Guide (2008) were also taken into account. SVMs was finally implemented using the pre-processed images (Section 3.1). In each classification performed, the γ parameter was set to a value equal to the inverse of the number of the spectral bands of the imagery used each time (i.e. in our study to 0.111 and 0.167 for ALI and TM respectively). The penalty parameter, which controls the trade-off between allowing training errors and forcing rigid margins, was set in to its maximum value (i.e. 100), as we were interested to create the most accurate possible model. The pyramid parameter was set to a value of zero, meaning that each image should be processed at full resolution. Finally a classification probability threshold of zero was applied forcing all image pixels to be classified into one class label and have no unclassified pixels in the imagery.

3.2.3. Artificial Neural Networks

ANNs is an artificial intelligence technique widely used in digital image analysis. An ANN consists essentially of a massively parallel distributed processor made up of simple processing units, which has a natural propensity for storing experiential knowledge and making it available for use (Haykin, 1994). A basic ANN model consists of an input layer, a hidden layer and an output layer. Nodes in the input layer represent variables used as input in the neural network which they could be spectral bands, textural features or other intermediate layers derived from remotely sensed image. In image classification the nodes in the output layer represent the classes where in each class will be one output node. The linkages between nodes represented weightings that lead the information flow through the network. Learning occurs by adjusting the weights in the node to minimize the difference between the output node activation and the real output, and the error is back propagated through the network and weight adjustment is made using a recursive method. ANNs implementation requires setting a number of parameters. These include the training rate, the training threshold contribution, the training momentum, the training RMS exit criteria field and the number of hidden layers to use and can choose between a logistic or hyperbolic activation function. Detailed descriptions of the definitions of those parameters can

be found elsewhere (Atkinson and Tatnall, 1997; Mas and Flores, 2008).

Herein, ANNs classifier was applied to both the ALI and TM acquired images using a multi-layered feed-forward ANN type based on logistic activation function available in ENVI. This technique uses standard back propagation for supervised learning. In both cases, a training threshold contribution value of 0.9, a training rate of 0.2, a training momentum of 0.9 and a training RMS exit criteria of 0.1 were used. The number of training iterations was set to 1000 and one hidden layer was used. The hidden layer configuration was determined by experimentation, as in other studies (e.g. Mas and Flores, 2008; Canty, 2009).

3.3. Accuracy assessment

The performance of the classifiers in turn applied to the two different satellite images and the significance of the results was thoroughly assessed in three ways, as described below.

3.3.1. Classification accuracy assessment using error matrices

Classification accuracy of the thematic maps was evaluated based on the computation of overall accuracy (OA), user's (UA), producer's (PA) accuracy and the Kappa (K_c) statistics (Congalton and Green, 1999). OA expresses as percentage (%) the probability that a pixel is classified correctly by the thematic map and is a measure of the overall classification accuracy. K_c measures the actual agreement between reference data and the classifier used to perform the classification versus the chance of agreement between the reference data and a random classifier. PA for a certain class expresses what percentage of a category on the ground is correctly classified by the analyst, and can define a measure of pixels omitted from its reference class (omission error). Likewise, UA expresses the percentage of pixels of a category that do not "truly" belong to the reference class, but are committed to other ground truth classes (commission error). In mathematical terms, these parameters are expressed as follows (Congalton and Green, 1999; Liu et al., 2007):

$$OA = \frac{1}{N} \sum_{i=1}^r n_{ii}, \tag{2}$$

$$PA = \frac{n_{ii}}{n_{icol}}, \tag{3}$$

$$UA = \frac{n_{ii}}{n_{irow}}, \tag{4}$$

$$K_c = N \sum_{i=1}^r n_{ii} - \sum_{i=1}^r \frac{n_{icol} n_{irow}}{N^2} - \sum_{i=1}^r n_{icol} n_{irow}, \tag{5}$$

where n_{ii} is the number of pixels correctly classified in a category; N is the total number of pixels in the confusion matrix; r is the number of rows; and n_{icol} and n_{irow} are the column (reference data) and row (predicted classes) total, respectively.

In computing the above statistical measures, approximately 44 validation points (i.e. pixels) from each class were selected directly from the ALI imagery (in total 212 pixels). The correspondence of the selected points to each class was further verified in the TM image. Validation points were generally selected in homogeneous regions and away from the locations where the training points had been collected, ensuring non-overlap of pixels between the training data and validation sites. To ensure consistency in our comparisons, the same set of validation points were used in evaluating the accuracy of all the thematic maps produced from the implementation of the different classifiers.

3.3.2. Statistical inference in classification accuracy

The statistical significance in the thematic maps accuracy between a pair of classifiers was further evaluated using the McNemar's test (Foody, 2004). This is a parametric, very simple to understand and execute statistical test that can be used in evaluating the superiority of one thematic map over another using the same validation sample, as was the case in the present study. The test is based upon the standardised normal test chi-square (χ^2) statistic computed from a two by two matrix based on correctly and incorrectly classified pixels in both classifications using Eq. (7) below (Foody, 2004; De Leeuw et al., 2006):

$$\chi^2 = \frac{(f_{12} - f_{21})^2}{f_{12} + f_{21}}, \quad (6)$$

where f_{12} denotes the number of cases that are correctly classified by classifier one but incorrectly classified by the classifier two, and f_{21} denotes the number of cases that are correctly classified by classifier two but wrongly classified by the classifier one (Manandhar et al., 2009). Thus, this test is focused on the binary distinction between correct and incorrect class allocations that are derived directly from the comparison of the error matrices between the two classifications compared. The derived χ^2 value from the implementation of this test is subsequently compared versus tabulated χ^2 values to indicate its statistical significance of the differences between the compared thematic maps products. The McNemar test was implemented herein three times, comparing the classification maps derived between the ALI and TM, for each classification technique applied. In our study, χ^2 values were compared for the 95% and 99% levels of confidence respectively.

3.3.3. Burnt area mapping accuracy assessment

Evaluation of the burnt area estimates was based on UA and PA statistics computed from the error matrix with reference to this specific class (Section 3.3.1). In addition, the burnt area map derived from each case was compared against the reference burnt area estimate acquired previously from SAFER. In this context, burnt area detection accuracy was evaluated following the rationale of Kontoes et al. (2009). Following this approach, accuracy of the burnt area detection was expressed in terms of detected area efficiency (DAE), skipped burnt area rate (SBA, omission error) and false burnt area rate (FBA, commission error). These accuracy figures were calculated on the basis of the following formulae:

$$\text{Detected area efficiency} = \frac{\text{DBA}}{\text{DBA} + \text{SBA}}, \quad (7)$$

$$\text{Skipped area rate} = \frac{\text{SBA}}{\text{DBA} + \text{SBA}}, \quad (8)$$

$$\text{False area rate} = \frac{\text{FBA}}{\text{DBA} + \text{FBA}}, \quad (9)$$

In the above equations, DBA is the Detected Burnt Area (common area between the generated burn scar polygon and the reference in situ polygon), FBA is the False Burnt Area (the area included in the generated burn scar polygon but not in the reference in situ polygon) and SBA is Skipped Burnt Area (the area included in the reference in situ polygon but not in the generated burn scar polygon). In order to enable overlay and facilitate efficiency in the burnt area comparisons, the burnt area estimates from ALI and TM were extracted from the corresponding classification maps and were subsequently transformed into vector format. The evaluation of the accuracy of the burnt area detection by this approach was performed in ArcGIS software platform (ESRI Inc., v. 9.3.1).

4. Results and discussion

Evaluation of both the land use/cover and burnt area estimates produced from the implementation of the different classifiers to the ALI and the TM imagery was subsequently carried out in a comparative manner. The main findings from our analysis are described and discussed next. For efficiency, first are presented the results concerning the overall land use/cover mapping classification accuracy of the thematic maps produced, followed by the burnt area mapping comparisons.

4.1. Overall classification

Classification maps derived from the implementation of the different classifiers to both the ALI and TM post-fire imagery are illustrated in Figs. 2 and 3 respectively. Table 2 summarises the various statistical parameters computed for evaluating the accuracy of the classification maps produced based on the error matrix. In overall OA and K_c results ranged from 86 to 95%, and from 0.829 to 0.937, respectively, signifying a high accuracy of all classification maps. In ALI classifications OA and K_c ranged from 91 to 95% and from 0.885 to 0.937 respectively, in comparison to the TM classifications where the same statistical parameters varied from 86 to 93.6% and from 0.829 to 0.920 respectively. Also, clearly, each classifier when combined with ALI produced higher OA and K_c results in comparison to when the same technique applied with TM data. On the basis of the OA and K_c results alone, is seen that ALI outperformed the TM sensor when the ML and the SVMs classifiers were applied, whereas the opposite occurred in the case of the ANNs. Also, SVMs when applied with either ALI or TM produced the highest classification results in comparison to all other classifiers.

UA and PA statistics for most classes were reported over 70%. This is suggesting a generally satisfactory performance of the classification techniques applied in mapping the individual land use/cover types. PA and UA of different classes in ALI classifications (73.5% and 83% respectively) were generally higher comparatively to those from TM (40% and 62% respectively). These results further support the previously reported finding that ALI has in general performed better in classifying the different land use/cover types in comparison to TM. Visual inspection of the derived thematic maps further supports the results of the statistical accuracy assessment; the maps appear similar in many regions, especially in large homogeneous areas (Figs. 2 and 3). However, there are discrepancies observed regionally, mainly evident in some linear structures of the "burnt area" class along the coastline as well as borders of the different land cover classes. Furthermore, noticeable land cover variations in the interior of the urban areas and of the south-west part of the study region for both sensors. These features are perhaps related to artefacts produced from the algorithms' implementation.

Evidently, for both ALI and TM, the classes with the highest mapping accuracy were those of the "burnt area" and the "forests class". On the other hand, all classifiers failed to clearly distinguish the classes "agricultural" and "semi-natural areas". Nevertheless, even for those two latter classes, high PA and OA were returned for most classifications applied, often above 70%. The high classification accuracy of both the "burnt area" and the "forests class" can be largely attributed to their distinct spectral signatures in comparison to the other classes. In comparison to a healthy and living vegetation a burnt area reflects comparatively more radiation in the visible (VIS) and shortwave infrared (SWIR) and absorbs radiation in the NIR, as a result of the destruction of the plant and leaf structure, vegetation (Yan et al., 2006; Kontoes et al., 2009). In addition, charcoal is strong absorber over the whole VNIR-SWIR spectrum, tough reflectance gradually increases with longer wavelengths. On the other, one possible reason for the lower and imbalanced accuracies of some classes such as the "agricultural" and "semi-natural

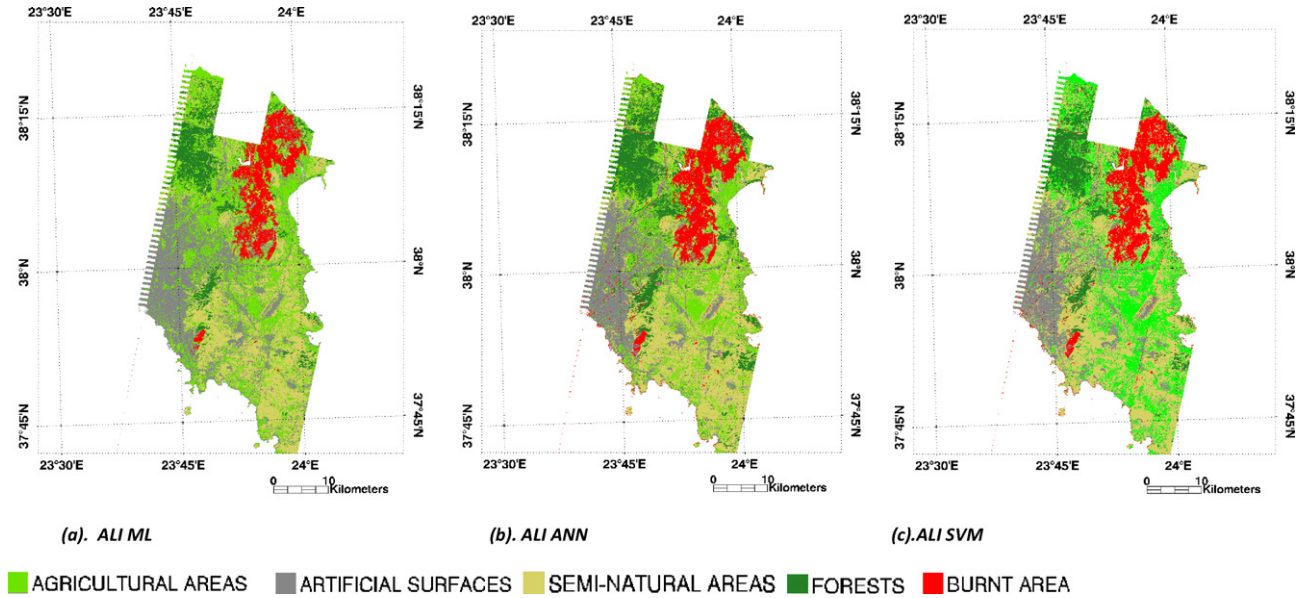


Fig. 2. The thematic maps derived from the Advanced Land Imager (ALI) imagery, using the Maximum Likelihood (ML) (a), Support Vector Machines (SVMs) (b) and Artificial Neural Networks (ANN) (c) classifiers. With the red colour is depicted the burnt area class. (For interpretation of the references to color in this figure legend, the reader is referred to the web version of this article.)

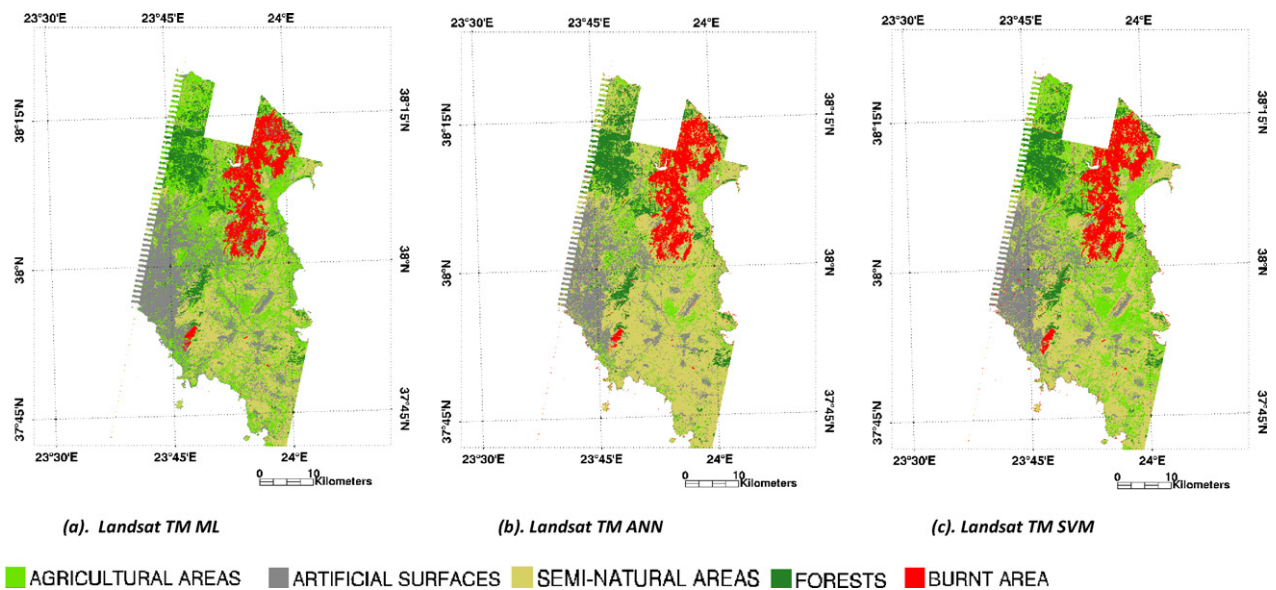


Fig. 3. The thematic maps derived from the Landsat Thematic Mapper (TM) imagery, using the Maximum Likelihood (ML) (a), Support Vector Machines (SVMs) (b) and Artificial Neural Networks (ANN) (c) classifiers. With the red colour is depicted the burnt area class. (For interpretation of the references to color in this figure legend, the reader is referred to the web version of this article.)

Table 2
Summary of the classification results obtained from the implementation of the different classifiers to the Advanced Land Imager (ALI) and Landsat Thematic Mapper (TM).

	Maximum Likelihood				Artificial Neural Networks				Support Vector Machines			
	Producer's accuracy (%)		User's accuracy (%)		Producer's accuracy (%)		User's accuracy (%)		Producer's accuracy (%)		User's accuracy (%)	
	ALI	TM	ALI	TM	ALI	TM	ALI	TM	ALI	TM	ALI	TM
Agricultural areas	73.47	59.18	85.71	100	75.51	40.82	94.87	100.00	81.63	73.47	95.24	100.00
Artificial surfaces	87.80	100.00	97.30	97.62	95.12	97.56	100.00	100.00	95.12	97.56	88.64	100.00
Forests	100.00	100.00	100.00	100.00	100.00	100.00	97.62	100.00	100.00	100.00	100.00	100.00
Semi-natural areas	97.56	100.00	83.33	73.21	100.00	100.00	87.23	62.12	100.00	100.00	91.11	82.00
Burnt area	97.78	97.78	100.00	100	100.00	100.00	100.00	100	100.00	100.00	100.00	100.00
Overall accuracy	90.78	90.32			93.58	86.18			94.93	93.55		
Kappa coefficient	0.885	0.879			0.920	0.829			0.937	0.920		

areas” might be related to the fact that in the field those classes had covered small areas and were often distributed in or around other land cover types. The latter, at the spatial resolution of 30 m of either ALI or TM can result to mixed pixels, which results to making it difficult to spectrally distinguish those classes with any of the pixel-based classifiers used herein. However, ALI showed an increased ability to spectrally discriminating the classes considered due to its higher number of spectral bands in comparison to TM. The statistical results of the spectral separability of the training points has also evidenced a lower separability between the agricultural and the semi-natural areas classes, in comparison to all other pairs of classes compared for both TM and ALI. Yet, ALI separability indices were higher than those of TM.

Results obtained clearly showed that the SVMs outperformed the other classifiers when combined with either ALI or TM image data. This appeared to be the case, at least in our study. The latter, can be accredited to a number of reasons. SVMs offer additional benefits in contrast to alternative classification models, as for example with ANNs or ML. SVMs have been designed to be able to identify an optimal separating hyperplane for classes' separation, which makes those classifiers resilient to getting trapped in local minima, as for example with ANNs. This is because of the convexity of the cost function which enables the classifier to consistently identify the global minimum, i.e. the optimal solution (e.g. Huang et al., 2002). As a result, SVMs are successful addressing ill-posed problems providing high classification accuracy results in comparison to other classifiers, even in cases when small training sets are used. An additional advantage of SVM is that their implementation does not require any assumption as regards the statistical distribution of the data to be classified, as for example is the case of the ML classifier implementation. This is particularly useful, since remotely sensed data follow usually unknown distributions (e.g. Mountrakis et al., 2011). The latter characteristic allows SVMs outperforming parametric classification techniques (such as ML applied here) because normality does not always give a correct assumption of the actual pixels distribution in each class (Su and Huang, 2009). In addition to the above, specifically the ML classifier is based on the assumption of only linear relationships between spectral data and class assignment (Friedl & Brodley, 1997 in Helmer et al., 2010), which is not always the case in nature. This can partially explain the ML lower classification accuracy in comparison to either SVMs or ANNs. Last but not least, in comparison to other machine learning classifiers (such as ANNs), SVMs implementation requires a small set of training points and a few only parameters need to be adjusted by the user. Yet, as a key limitation of all the classifiers employed herein could be accounted the fact that those do not operate on a sub-pixel level. The latter, can result to misclassification errors occurred due to possible pixel mixture problems and can be particularly evident when coarse spatial resolution data is used.

ALI and TM have similar spatial resolution, which indicates practically the same mapping scale. However, differences were clearly observed in the classification results for each classifier implementation, with the ALI classification outperforming – marginally in some cases – that of TM (Table 2). The latter can be largely attributed to the differences between the two sensors technical specifications, specifically the contribution of additional bands as well as the higher signal to noise ratio and increased dynamic range of ALI in comparison to TM. This finding is in agreement to other studies comparing ALI capability comparatively to Landsat TM/ETM+ in various applications including land use/cover. Such studies have also underlined that that ALI improved dynamic range and signal-to-noise ratio, and additional multispectral bands can provide an enhanced capability for studying land use/land cover characteristics and its changes (Thenkabail et al., 2004; Neuenschwander et al., 2005; Pu et al., 2005; Deller, 2006; Helmer et al., 2010).

The statistical significance of the differences observed between classifier-sensor pairs was investigated by applying the McNemar non-parametric test at statistical significance 95% and 99% confidence levels (Table 3). Results showed that differences in the ML classification between ALI and TM were found significant at 95% confidence level. On the other, the differences in the classification results for the case of SVMs and ANNs implementation were found significant at 99% confidence level. The above results further supported the argument stated previously that the presence of the additional spectral bands and higher SNR of ALI image data assisted in improving somehow the overall classification accuracy.

Last but not least, our classification accuracy results agree to those reported in previous studies also examining land use/cover mapping using ALI data. For example, Neuenschwander et al. (2005) performed a comparative study between ALI and ETM+ in land cover mapping for a region in Okavango Delta, Africa. Authors applied the Bayesian Pairwise pixel-based classifier (Crawford et al., 1999) for mapping land cover and reported consistently higher classification accuracy by ALI in comparison to ETM+ with OA and kappa ranging from 75 to 81% and 0.737 to 0.798 respectively. In another work, Thenkabail et al. (2004) compared the performances of four sensors (namely Hyperion, IKONOS, ALI, and ETM+) for mapping rainforest in southern Cameroun in Africa. Authors reported low OA accuracies in classifying nine complex rainforest classes ranging from 42 to 51%, with ALI exhibiting the highest performance among the broadband sensors. To our knowledge, no other investigations have been concerned with the evaluation of ALI in land use/cover mapping by image classification. As regards the classification results from the TM sensor, our results agree favourably to findings from previous works conducted, reporting generally higher classification performance by SVMs in comparison to ANNs (e.g. Nemmour and Chibani, 2006; Dixon and Candade, 2008).

4.2. Burnt area mapping

Of special interest is the evaluation of the burnt area retrievals from the combination of the different classifiers with the co-orbital ALI and TM post-fire imagery acquired shortly after the fire suppression. Apart from the evaluation on the basis of the error matrix statistics (UA, PA – Table 2), the classified burnt areas were assessed against the validated burnt area estimate from SAFER operational service (Table 4). A visual observation of the spatial agreement of the burnt area estimates illustrated in Figs. 4 and 5 indicates that all classifications returned a generally similar burn scar shape, close to that mapped by the reference polygon from SAFER. The latter is suggestive of a generally high-quality spatial agreement between the compared datasets. The commonly identified burnt area between the output and SAFER dataset is depicted in green colour, and is high for the comparisons performed in all cases. Clearly, for both ALI and TM burnt area mapping results, with respect to SAFER estimate, higher omission (in red) and commission errors (in cyan) appear in the burn scar derived from the implementation of the ML and ANN methods, in comparison to that from the SVMs.

In terms of absolute accuracy, all classifications carried out returned results in close agreement to the SAFER estimate. Absolute differences in burnt area estimate between SAFER and ALI ranged from 8.24 to 17.53% and between SAFER and TM between 8.4% and 17.5%. Noticeably, highest agreement in the total burnt area estimates was generally observed in the case of SVMs implementation (~8% difference from SAFER), followed by ANNs (~11% difference from SAFER) and finally ML classifiers (~15% difference from SAFER).

As in Kontoes et al. (2009), a further set of statistical parameters were computed to quantitatively evaluate the ability of the different classifiers in predicting burnt area in comparison to the reference estimate from SAFER (Table 4). Results showed that the

Table 3
McNemar test results for the case of the different classifiers compared herein between ALI and TM.

Classification method	f_{11}	f_{12}	f_{21}	f_{22}	Total	Chi-square (χ^2)	p-Value
Maximum Likelihood	179	16	6	11	212	6.55	<0.05
Artificial Neural Networks	186	17	2	7	212	11.84	<0.001
Support Vector Machines	188	18	1	5	212	15.21	<0.001

f_{11} : number of cases with correct classification in both maps; f_{12} : number of cases that are correctly classified by ALI but incorrectly by TM; f_{21} : number of cases that are correctly classified TM, but incorrectly by ALI; f_{22} : number of cases that are wrongly classified by both ALI and TM.

Table 4
Summary of the burnt area comparisons between SAFER and those derived from the implementation of the different classifiers to the ALI and Landsat-TM images.

Classification method tested	Common burnt area between prediction & SAFER (DBA)	False burnt areas (FBA)	Skipped burnt areas (SBA)	Detection efficiency rate (%) [DBA/(DBA + SBA)]	Commission error (false alarm rate) (%) [FBA/(DBA + FBA)]	Omission error (%) [SBA/(DBA + SBA)]
ALI.ML	104.15	18.68	22.14	0.825	0.152	0.208
ALI.ANN	113.89	27.65	12.41	0.902	0.195	0.098
ALI.SVM	115.89	23.14	10.50	0.917	0.166	0.083
TM.ML	110.44	16.23	15.86	0.874	0.128	0.126
TM.ANN	113.29	20.68	13.00	0.897	0.154	0.102
TM.SVM	115.79	23.14	10.50	0.917	0.167	0.083

highest burnt area detection efficiency rate (DBA) observed for the case of SVMs classifier implementation, followed by ANNs and ML. This appeared to be the case in both ALI and TM classifications. Similarly, skipped burnt area (SBA, omission error) was also lowest in the case of SVMs in comparison to the other classifiers for both ALI and TM results. Yet, in terms of falsely detected burnt area (FBA, commission error), no clear trends in observations could be

noticed, apart from the fact that the ML results had the lowest FBA reported for both ALI and TM.

Differences in the burnt area estimates can be attributed to several factors. Variations in the principles that govern the classifiers operation that result to exploiting differently the spectral information content of the burnt area recorded by each sensor can in part explain the differences in the results obtained (Giglio et al., 2006).

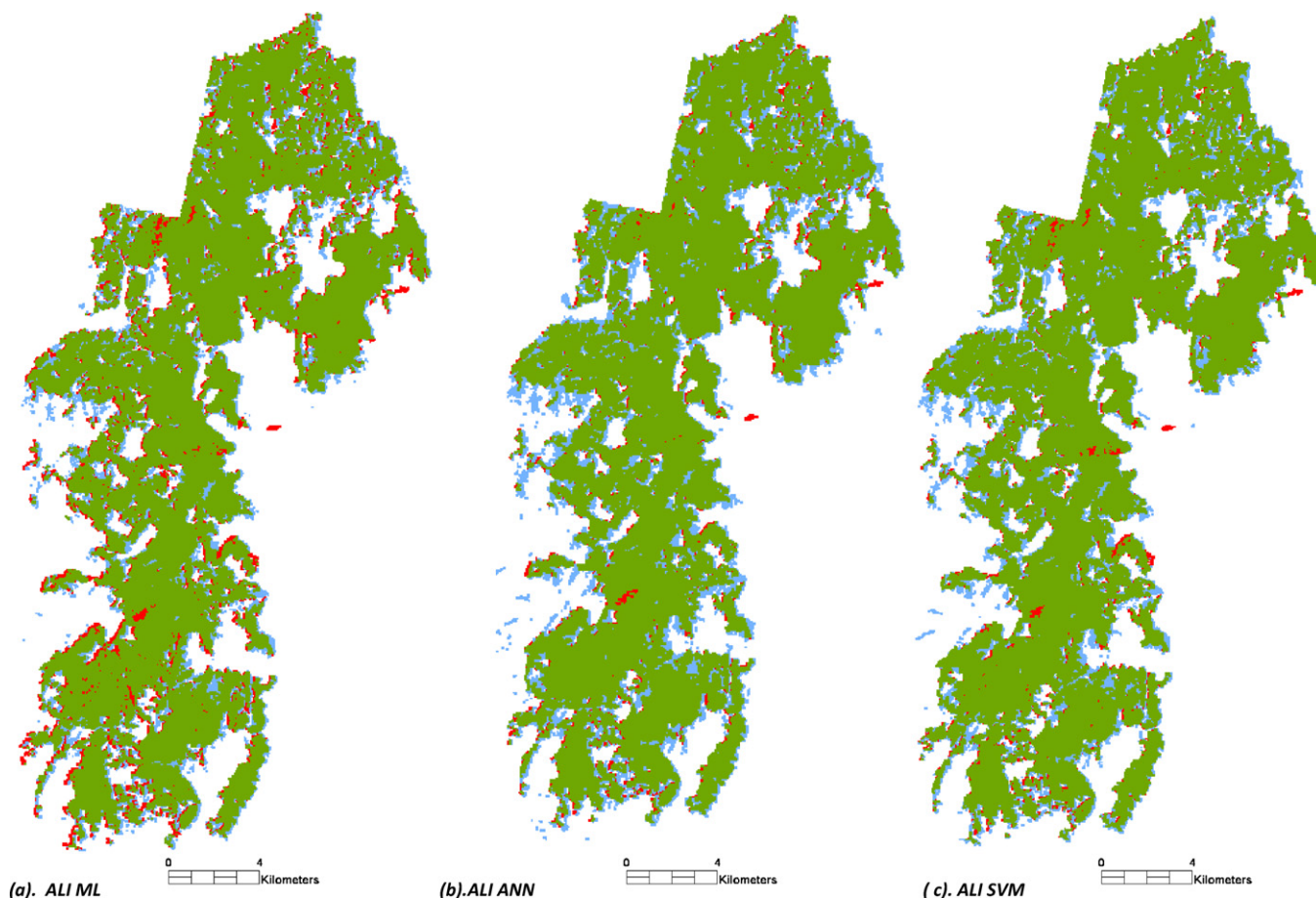


Fig. 4. Comparisons of the burnt area estimates derived from the combined use of Advanced Land Imager (ALI) sensor with the different classifiers applied, versus those from SAFER. It is shown the commonly identified burnt area between ALI and SAFER (green), the burnt area identified only by SAFER (red) and the burnt area identified only by ALI (cyan). (For interpretation of the references to color in this figure legend and in text, the reader is referred to the web version of this article.)

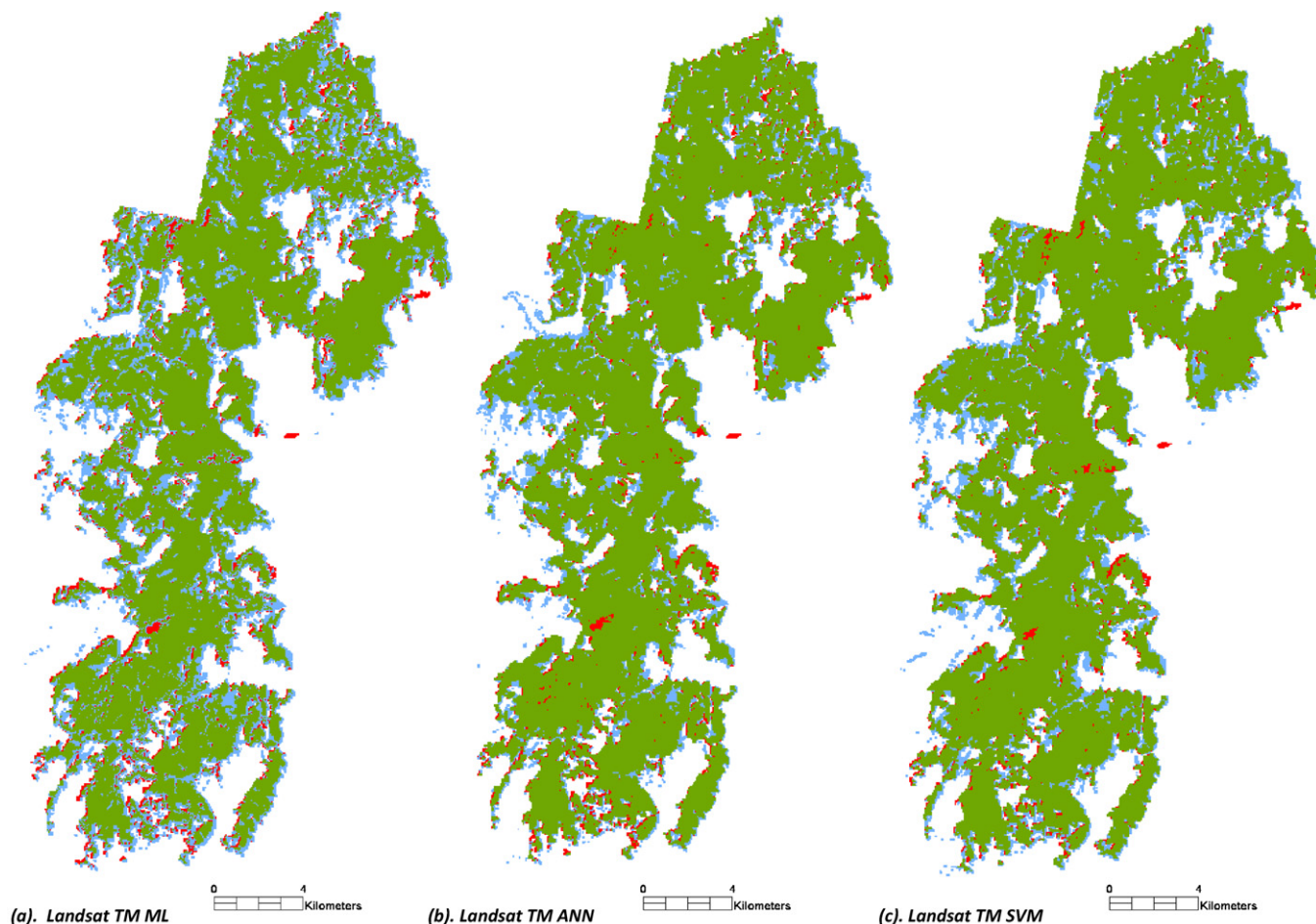


Fig. 5. Comparisons of the burnt area estimates derived from the combined use of Landsat Thematic Mapper (TM) with the different classifiers applied, versus those from SAFER. It is shown the commonly identified burnt area between TM and SAFER (green), the burnt area identified only by SAFER (red) and the burnt area identified only by TM (cyan). (For interpretation of the references to color in this figure legend and in text, the reader is referred to the web version of this article.)

Findings from our work suggest that application of SVMs to ALI or TM produces the highest burnt area delineation accuracy. Previous studies using different types of satellite datasets have also demonstrated the superiority of SVMs over other classifiers for burnt area extraction (Cao et al., 2009; Petropoulos et al., 2011a). Discrepancies in the burnt area estimates can also increase with increasing heterogeneity of the burned surface, as is the case in Mediterranean landscapes. In addition, shaded surfaces present in terrains of high topography variation, as is the case of many Mediterranean landscapes, may cause spectral confusion resulting to pixel misclassification and subsequent overestimation of burnt areas (Tanaka et al., 1983; Sedano et al., 2011). Finally, differences in the spectral and sensor technologies between different remote sensing radiometers, as in our case, can also partially explain differences in the burnt area estimates even when the same technique is used (Eva and Lambin, 2000; Boschetti et al., 2004). Our results show that the benefit from the ALI use in burnt area extraction appears to be its higher number of spectral SWIR bands in combination to its higher SNR. In agreement with previous studies specifically the presence of the additional SWIR bands assists in better detection capability of the burnt area spectral responses of different land surface objects. Roy et al. (2008) using MODIS data demonstrated that for several types of ecosystems the highest spectral separability of burnt area corresponded to the near infrared (841–876 nm) and short wave infrared bands (1230–1250 nm). Since only ALI has a band (band 5p) in this shortwave infrared region, this results to an increased burn scar detection capability of the sensor in comparison to TM.

Authors in the same study showed that lack of shortwave infrared band in this spectral region imposes potentially a limitation in burnt area detection capability of a sensor since vegetation senescence or removal can result in similar near infra red reflectance than burned scars. Thus, all in all, SVMs due to their technical characteristics in comparison to other classifiers were able to better exploit the ALI advanced spectral configuration characteristics, producing more accurate results in burnt area extraction.

5. Conclusions

The aim of our study was to evaluate the capability of ALI with respect to Landsat TM for land cover mapping and burnt area delineation, when combined with different pixel-based classification techniques. ML, ANNs and SVMs classifiers were parameterised and subsequently applied to the acquired images. As a case study we used a Mediterranean fire event that occurred close to the capital of Greece in summer 2009. Both ALI and TM images were acquired shortly after the fire.

The classification results demonstrated that any pair of classifier-sensor returned acceptable land use/cover and burnt area maps. However, one pair, namely SVMs-ALI, provided marginally, yet statistically significant, higher accuracy. SVMs proved capable of taking advantage of the ALI's improved technical specifications. The latter, allowed SVMs to deal more efficiently with the landscape structure complexities of our study site in comparison to the other classifiers tested. From an algorithmic perspective, these

findings consist a serious motivation and promise for future advances in terms of the SVMs algorithm development in the context of the development of the future Landsat 8 mission for which ALI has been specifically developed.

All in all, our study opens new perspectives in burnt area mapping, as this is the first study bringing concrete evidence with respect to the capability of ALI radiometer for accurate burnt area detection and delineation. ALI sensor, as its predecessor, the TM, satisfies the needs for low-cost, rapid, accurate, regional mapping of burnt areas.

Acknowledgements

Authors gratefully acknowledge the United States Geological Survey (USGS) for providing free access to the Landsat TM and the EO-1 ALI satellite images. We are also grateful to the anonymous reviewers for their constructive comments that helped to significantly improve the manuscript.

References

- Atkinson, P.M., Tatnall, A.R., 1997. Introduction: neural networks in remote sensing. *International Journal of Remote Sensing* 18, 699–770.
- Boschetti, L., Eva, H.D., Brivio, P.A., Gregoire, J.M., 2004. Lessons to be learned from the comparison of three satellite-derived biomass burning products. *Geophysical Research Letters* 31, L21501.
- Canty, M.J., 2009. Boosting a fast neural network for supervised land cover classification. *Computers and Geosciences* 36 (6), 1280–1295.
- Cao, X., Chen, J., Matsushita, B., Imura, H., Wang, L., 2009. An automatic method for burn scar mapping using support vector machines. *International Journal of Remote Sensing* 30 (3), 577–594.
- Castillejo-Gonzalez, I.L., Lopez-Granados, F., Garcia-Ferrer, A., Pena-Barragan, J.M., Jurado-Exposito, M., De la Orden, M.S., Gonzalez-Audican, M., 2009. Object- and pixel-based analysis for mapping crops and their agro-environmental associated measures using QuickBird imagery. *Computers and Electronics in Agriculture* 68, 207–215.
2012. CEOS Earth Observation Handbook, CEOS Missions, Instruments and Measurements database online <http://database.eohandbook.com/> (accessed 13.01.12).
- Chen, S., Fang, L., Zhang, L., Huang, W., 2009. Remote sensing of turbidity in seawater intrusion reaches of Pearl River Estuary – a case study in Modaomen water way, China. *Estuarine, Coastal and Shelf Science* 82, 119–127.
- Congalton, R., Green, K., 1999. Assessing the Accuracy of Remotely Sensed Data: Principles and Practices. CRC/Lewis Press, Boca Raton, FL, pp. 137.
- Crawford, M.M., Kumar, S., Ricard, M.R., Gibeaut, J.C., Neuenschwander, A.L., 1999. Fusion of airborne polarimetric and interferometric SAR data for classification of coastal environments. *IEEE Transactions on Geoscience and Remote Sensing* 37, 1306–1315.
- Datt, B., McVicar, T.R., Van Niel, T.G., Jupp, D.L.B., Pearlman, J.S., 2003. Pre-processing EO-1 Hyperion hyperspectral data to support the application of agricultural indexes. *IEEE Transactions on Geoscience and Remote Sensing* 41, 1246–1259.
- De Leeuw, J., Jia, H., Yang, L., Liu, X., Schmidt, K., Skidmore, A.K., 2006. Comparing accuracy assessments to infer superiority of image classification methods. *International Journal of Remote Sensing* 27, 223–232.
- Deller, M.E.A., 2006. Facies discrimination using Landsat Thematic Mapper, ASTER and ALI data – examples from Eritrea and Arabia. *International Journal of Remote Sensing* 27 (12), 2389–2409.
- Dixon, B., Candade, N., 2008. Multispectral land use classification using neural networks and support vector machines: one or the other, or both? *International Journal of Remote Sensing* 29 (4), 1185–1206.
- ENVI User's Guide, 2008. ENVI on-line software user's manual, ITT Visual Information Solutions.
- Eva, H., Lambin, T., 2000. Fires and land-cover change in the tropics: a remote sensing analysis at the landscape scale. *Journal of Biogeography* 27 (2000), 765–776.
- FAO, 2001. Global Forest Fire Assessment 1990–2000. Forest Resources Assessment Programme, Working Paper No. 55, 2001. <http://www.fao.org/forestry/fo/fra/docs/Wp55_eng.pdf> (accessed 14.04.11).
- Footy, G.M., 2004. Thematic map comparison: evaluating the statistical significance of differences in classification accuracy. *Photogrammetric Engineering & Remote Sensing* 70 (5), 763–767.
- Friedl, M.A., Brodley, C.E., 1997. Decision tree classification of land cover from remotely sensed data. *Remote Sensing of Environment* 61, 399–409.
- Giglio, L., Csizsar, I., Justice, C.O., 2006. Global distribution and seasonality of active fires as observed with the Terra and Aqua MODIS sensors. *Journal of Geophysical Research—Biogeosciences* 111, G02016.
- Haykin, S., 1994. *Neural Networks*. Macmillan College Publishing Company, Inc., New York.
- Helmer, E.H., Ruzycycki, T.S., Wunderle, J.M., Vogesser, S., Rufenacht, B., Kwit, C., Brandeis, T.J., Ewert, D.N., 2010. Mapping tropical dry forest height, foliage height profiles and disturbance type and age with a time series of cloud-cleared Landsat and ALI image mosaics to characterize avian habitat. *Remote Sensing of Environment* 114, 2457–2473.
- Huang, C., Davis, L.S., Townshend, J.R.G., 2002. An assessment of support vector machines for land cover classification. *International Journal of Remote Sensing* 23, 725–749.
- Huang, C., Song, K., Kim, S., Townshend, J.R.G., Davis, P., Masek, J.G., Goward, S.N., 2008. Use of dark object concept and support vector machines to automate forest cover change analysis. *Remote Sensing of Environment* 112, 970–985.
- Hubbard, B.E., Crowley, J.K., 2005. Mineral mapping on the Chilean-Bolivian Altiplano using co-orbital ALI, ASTER and Hyperion imagery: data dimensionality issues and solutions. *Remote Sensing of Environment* 99, 173–186.
- Kokaly, R.F., Rockwell, B., Haire, W., King, S.L., 2007. Characterisation of post-fire surface cover, soils and burn severity at the Cerro Grande Fire, New Mexico, using hyperspectral and multispectral remote sensing. *Remote Sensing of Environment* 106, 305–325.
- Kontoes, C.C., Poilve, H., Florsch, G., Keramitsoglou, I., Paralikidis, S., 2009. A comparative analysis of a fixed thresholding vs. a classification tree approach for operational burn scar detection and mapping. *International Journal of Applied Earth Observation and Geoinformation* 11, 299–316.
- Kuemmerle, T., Chaskovskyy, O., Knorn, J., Radeloff, V.C., Krühlov, I., 2009. Forest cover change and illegal logging in the Ukrainian Carpathians in the transition period from 1988 to 2007. *Remote Sensing of Environment* 113, 1194–1207.
- Li, D.-C., Liu, C.-W., 2010. A class possibility based kernel to increase classification accuracy for small data sets using support vector machines. *Expert Systems with Applications* 37, 3104–3110.
- Liu, C., Frazier, P., Kumar, L., 2007. Comparative assessment of the measures of thematic classification accuracy. *Remote Sensing of Environment* 107, 606–616.
- Lu, D., Weng, Q., 2007. A survey of image classification methods and techniques for improving classification performance. *International Journal of Remote Sensing* 28, 823–870.
- Mendenhall, J.A., Lencioni, D.E., Parker, A.C., 1999. Radiometric calibration of the EO-1 Advanced Land Imager SPIE Conference on Earth Observing Systems IV. *International Society for Optical Engineering* 3750, 117–131.
- Manandhar, R., Odeh Inakwu, O.A., Ancey, T., 2009. Improving the accuracy of land use and land cover classification of Landsat data using post-classification enhancement. *Remote Sensing* 1 (3), 330–344.
- Mas, J.F., Flores, J.J., 2008. The application of artificial neural networks to the analysis of remotely sensed data. *International Journal of Remote Sensing* 29, 617–663.
- Mathur, A., Foody, G.M., 2008. Crop classification by support vector machines with intelligently selected training data for an operational application. *International Journal of Remote Sensing* 29 (8), 2227–2240.
- Mountrakis, G., Im, J., Ogole, C., 2011. Support vector machines in remote sensing: a review. *ISPRS Journal of Photogrammetry and Remote Sensing* 66, 247–259.
- Nemmour, H., Chibani, Y., 2006. Multiple support vector machines for land cover change detection: an application for mapping urban extension. *ISPRS Journal of Photogrammetry and Remote Sensing* 61, 125–133.
- Neuenschwander, A., Crawford, M.M., RinkGrose, S., 2005. Results from the EO-1 experiment – a comparative study of Earth Observing-1 Advanced Land Imager (ALI) and Landsat ETM+ data for land cover mapping in the Okavango Delta, Botswana. *International Journal of Remote Sensing* 26, 4321–4337.
- Otukei, J.R., Blaschke, T., 2010. Land cover change assessment using decision trees, support vector machines and maximum likelihood classification algorithms. *International Journal of Applied Earth Observation and Geoinformation* 12S, S27–S31.
- Pengra, B.W., Johnston, C.A., Loveland, T.R., 2007. Mapping and invasive plant, *Phragmites australis*, in coastal wetlands using EO-1 Hyperion hyperspectral sensor. *Remote Sensing of Environment* 108, 74–81.
- Petropoulos, G., Knorr, W., Scholze, M., Boschetti, L., Karantounias, G., 2010a. Combining ASTER multispectral imagery analysis and support vector machines for rapid and cost-effective post-fire assessment: a case study from the Greek fires of 2007. *Natural Hazards and Earth Systems Science* 10, 305–317.
- Petropoulos, G., Vadrevu, K.P., Xanthopoulos, G., Karantounias, G., Scholze, M., 2010b. A comparison of spectral angle mapper and artificial neural network classifiers combined with Landsat TM imagery analysis for obtaining burnt area mapping. *Sensors* 10, 1967–1985.
- Petropoulos, G., Kontoes, C., Keramitsoglou, I., 2011a. Burnt Area Delineation from a uni-temporal perspective based on Landsat TM imagery classification using Support Vector Machines. *International Journal of Applied Earth Observation and Geoinformation* 13, 70–80, doi:10.1016/j.jag.2010.06.008.
- Petropoulos, G.P., Kalaitzidis, C., Vadrevu, K.P., 2011b. Support vector machines and object-based classification for obtaining land use/cover cartography from hyperion hyperspectral imagery. *Computers and Geosciences*, in press, doi:10.1016/j.cageo.2011.08.019.
- Pimstein, A., Eitel, J.U.H., Long, D.S., Mufradi, I., Karnieli, A., Bonfil, D.J., 2009. A spectral index to monitor the ehad-emergence of wheat in semi-arid conditions. *Fields Crops Research* 111, 218–225.
- Pu, R., Gong, P., Biging, G.S., 2005. EO-1 Hyperion and Landsat 7 ETM+ data comparison for estimating forest crown closure and leaf area index. *International Journal of Remote Sensing* 26, 457–474.
- Quintano, C., Fernandez-Manso, A., Fernandez-Manso, O., Shimabukuro, Y.E., 2006. Mapping burnt areas in Mediterranean countries using spectral mixture analysis

- from a uni-temporal perspective. *International Journal of Remote Sensing* 27 (4), 645–662.
- Richards, J.A., 1999. *Remote Sensing Digital Image Analysis*. Springer-Verlag, Berlin, p240.
- Roy, D.P., Boschetti, L., 2009. Southern Africa Validation of the MODIS, L3JRC and GlobCarbon Burned Area Products. *IEEE transactions on Geoscience and Remote Sensing* 47 (4), 1032–1044.
- Roy, D.P., Boschetti, L., Justice, C.O., Ju, J., 2008. The collection 5 MODIS burned area product – global evaluation by comparison with the MODIS active fire product. *Remote Sensing of Environment* 2008 112, 3690–3707.
- Sedano, F., Kempeneers, P., Strobl, P., Vogt, P., Seebach, L., San Miguel, J.A., 2011. Cloud mask 15 methodology for high resolution remote sensing data combining information from high and 16 medium resolution optical sensors. *ISPRS Journal of Photogrammetry and Remote Sensing* 66, 588–596.
- Sifakis, N.I., Iossifidis, C., Kontoes, C., Keramitsoglou, I., 2011. Wildfire detection and tracking over Greece using MSG-SEVIRI satellite data. *Remote sensing* 3, 524–538.
- Silva, J.M.N., Sa, A.C.L., Pereira, J.M.C., 2005. Comparison of burnt area estimates derived from SPOT-VEGETATION and Landsat ETM+ data in Africa: influence of spatial pattern and vegetation type. *Remote Sensing of Environment* 96, 188–201.
- Su, L., Huang, Y., 2009. Support vector machine (SVMS) classification: comparison of linkage techniques using a clustering-based method for training data selection. *GIScience & Remote Sensing* 46 (4), 411–423.
- Tanaka, S., Kimura, H., Suga, Y., 1983. Preparation of a 1:25 000 Landsat map for assessment of burnt area on Etajima Island. *International Journal of Remote Sensing* 4, 17–31.
- Thenkabail, P.S., Enclona, E.A., Ashton, M.S., Legg, C., Dieu, M.J.D., 2004. Hyperion, IKONOS, ALI and ETM+ sensors in the study of African rainforests. *Remote Sensing of Environment* 90, 23–43.
- Ungar, S.G., Pearlman, J., Mendenhall, J.A., Reuter, D., 2003. Overview of the Earth Observing-1 (EO-1) mission. *IEEE Transactions on Geoscience and Remote Sensing* 41, 1149–1159.
- Vapnik, V., 1995. *The Nature of Statistical Learning Theory*. Springer-Verlag, New York, NY.
- Yan, G., Mas, J.-F., Maathuis, B.H.P., Xiangmin, Z., van Dijk, P.M.O., 2006. Comparison of pixel-based and object-oriented image classification approaches – a case study in a coal fire area, Wuda, Inner Mongolia, China. *International Journal of Remote Sensing* 27 (12), 4039–4055.